Millimeter-wave slotted waveguide array with unequal beamwidths and low sidelobe levels for vehicle radars and communications

Qin, Liting; Lu, Yunlong; You, Qingchun; Wang, Yi; Huang, Jifu; Gardner, Peter

Document Version
Peer reviewed version

Link to publication on Research at Birmingham portal

Millimeter Wave Slotted Waveguide Array with Unequal Beam-widths and Low Sidelobe Levels for Vehicle Radars and Communications

Liting Qin, Yunlong Lu, Qingchun You, *Student Member, IEEE,* Yi Wang, *Senior Member, IEEE*, Jifu Huang and Peter Gardner, *Senior Member, IEEE*

Abstract—A low profile, high gain 32×64-slot array antenna with unequal beam-width in the E- and H-planes and low sidelobe is proposed for vehicular applications in the 71–81 GHz band. The antenna is composed of 512 (16×32) 2×2-slot subarrays arranged with equal spacing and excited by a non-uniform corporate-feed-network. A 2-D amplitude-tapering (complying with Taylor distribution) is used to achieve the low sidelobe level (SLL). Combined with the different dimensions of the array, the sidelobes and the beam-widths in the E- and H-plane are independently controlled. A prototype slotted waveguide (SW) array is fabricated to verify the array properties. Measurements show that the matching of the array is better than -14 dB over the entire bandwidth. The first SLL is lower than -18.9 dB/-24 dB with the maximum 3-dB beam-width of 2.3°/1.3° in the E- and H-plane, respectively. The peak gain of over 39.4 dBi and the cross-polarization of below -36.2 dB are also achieved. The demonstrated features of high-gain, low SLL, and independent controllability of the beam in the E- and H-plane are most desirable for vehicular communications and radars.

Keywords—*Slotted waveguide array, Low sidelobe, High gain, 2-D amplitude-tapering.*

I. INTRODUCTION

Radars and communication systems in automobiles, unmanned aerial vehicles have undergone rapid development in recent years [1]. 77 GHz radars have become the main stream technology [2]. Different field of views are required for different detection scenarios. For the long range automotive radar, the expected detection range is around 200 m, and the beam-widths in the azimuth / elevation plane are normally suppressed into no more than ±2°/±5°, which enhances the radar resolution [1]. In unmanned aerial vehicle applications, the beam-widths in azimuth/elevation plane are also usually unequal and even narrower. Additionally, no matter what kind of radar application, it is often highly desirable to have a low side-lobe-level (SLL) to minimize the effect of clutter and interference [3], [4]. So, it is crucially important to be able to control the beams in both the azimuth and elevation planes.

Apart from vehicle radars, millimeter wave (MMW) is also considered one of the key enabling technologies for vehicular communications [5]-[8]. The E-band (71-76 GHz and 81-86 GHz), next to the popular radar band of 76-81 GHz, has attracted a lot of attention for communication systems [9], [10]. In this work, we choose the frequency range of 71-81 GHz to cover the interest from both radars and E-band communications. We aim to demonstrate the capability of an antenna platform that addresses the design challenges of high gain, low sidelobe, low profile, and independently controllable beam-width in the E- and H- plane.

Weighting the power applied to the array elements (the so-called amplitude tapering) is one major approach used to reduce sidelobes [11]. The weighting normally takes one of three distributions: Binomial, Chebyshev and Taylor [12]-[15]. Binomial distribution could eliminate all sidelobes but increases the beam-width. Chebyshev distribution offers the narrowest beam width under the same array sizes and SLL. However, the physical implementation of this distribution is very challenging as it requires large variation of the power amplitudes and therefore power dividers with large power ratios. Taylor distribution renders less amplitude variation and the feed network is easier to implement. It is still very effective in suppressing the sidelobes. Taylor distribution has been the choice of many previous works. Most of them were based on microstrip feed networks [16]-[19]. At MMW band, however, the losses of microstrip feed are relatively high for a high gain antenna. Since waveguide has much lower losses, waveguide-based arrays have been a top choice for high performance MMW antennas. Among them are slotted waveguide (SW) arrays [20], [21] and continuous transverse stub (CTS) arrays [22]. The realization of amplitude tapering in waveguide structures is a more involved design challenge and very few works have been reported in the literature. One waveguide-based Taylor distribution feed network that the authors are aware of is a 15 GHz 16×16 SW array antenna, with a SLL of -22 dB [23]. It was a square array with the same beam characteristics in the E- and H-plane. Other techniques have also been demonstrated to reduce the SLL, for instance, by devising a 45° linearly polarized array antenna [24]. This reduces the sidelobes without affecting the gain and beam-width. Nevertheless, it still has large sidelobes in the radiation
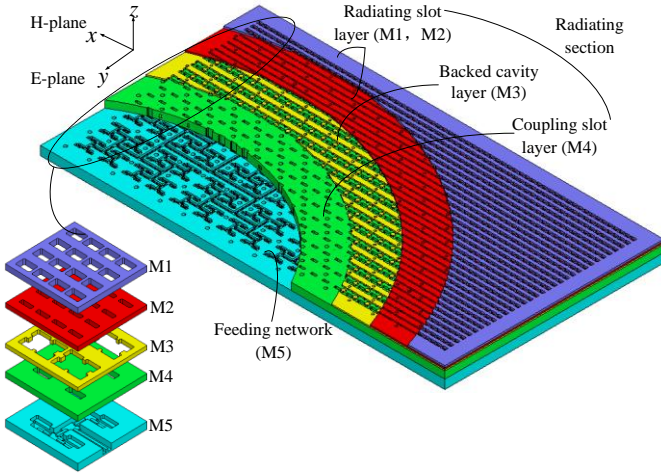
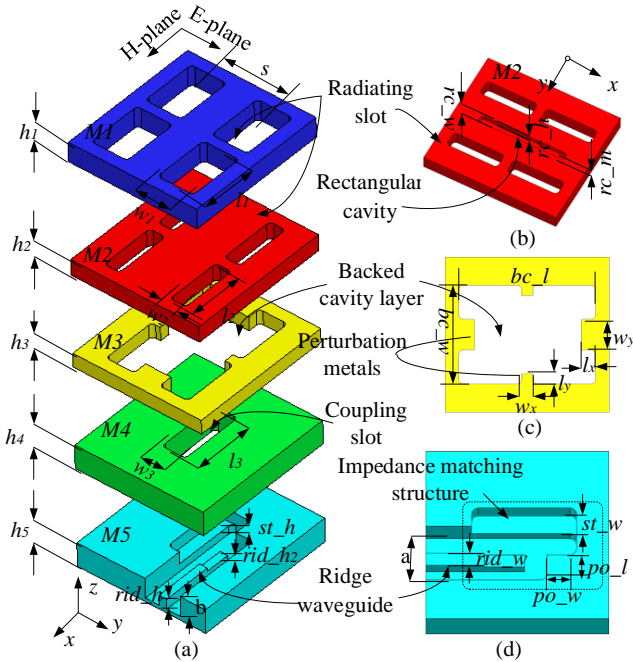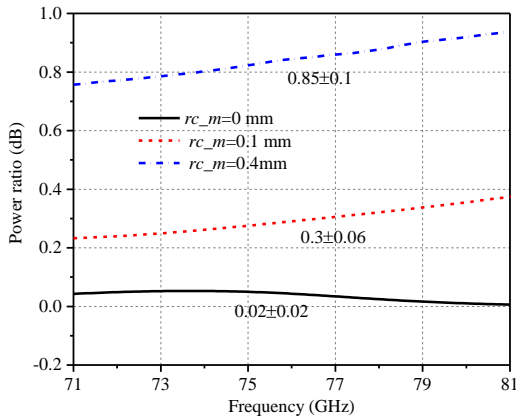Fig. 1. Configuration of the 32×64-slot antenna array.

Fig. 2. (a) Configuration of the 2×2-slot subarray; (b) Underside view of the radiating slot layer M2; (c) Backed cavity; (d) Ridge waveguide.

Fig. 3. Effect of the trench offset (rc_m) on the power ratio achieved between the two slots of the subarray in the E-plane.

patterns, although they are not at the same planes of main

polarization.

In this paper, based on amplitude-tapering of a Taylor distribution, a low profile, high gain 32×64-slot array antenna with unequal beam width in the E- and H-plane and low sidelobes is presented. A set of equal-phase and unequal power dividers based on single-ridge waveguides are employed to form the 2-D amplitude-tapering feed network. Combined with different dimensions of the array along the x- and y-axis, radiation patterns of low sidelobes and unequal beam-width in the E- and H-plane are achieved. To validate the design concept, a prototype operating at 71-81 GHz is fabricated and measured. All the simulations are carried out with HFSS.

II. SW ARRAY DESIGN AND ANALYSIS

A. Configuration of the array

The configuration of the 32×64-slot antenna array is shown in Fig. 1. It contains five layers from top to bottom, namely M1, M2, M3, M4 and M5. The coupling slot layer (M4), backed cavity layer (M3) and radiating slot layers (M1, M2) constitute the radiation section, whereas the feed network is in layer M5. The subarray (based on the design in [25]) is a 2×2-slot and works as the basic radiation unit. 16×32 subarrays are arranged in the x- and y-directions with equal spacing in layer M1 and M2. It should be noted that, different from [23] and [25], two stacked layers (M1 and M2) of different slot sizes are used to increase the operating bandwidth. A 16×32 2-D power divider network is in the bottom layer (M5). The operation mechanism is as follows: the power is coupled from the feed network (M5) to the back cavities (M3) through the coupling slots (M4). Each backed cavity excites one 2×2 subarray in M2 which radiates from M1 into free space.

As the number of subarray in the x-direction is twice the number in the y-direction, different beam-widths are achieved in the E- and H-plane. Combined with the 2-D Taylor synthesis, the radiation performance (3-dB beam-width and SLL) in the E- and H-plane can be controlled independently, which is an attractive feature for vehicular communications and radars.

B. 2×2-slot subarray

The detailed view of one 2×2-slot subarray is shown in Fig. 2(a). The different widths (w_1 and w_2) of the radiating slots in M1 and M2 work as a two-section impedance transformer, which is designed to increase the bandwidth [26]. The spacing (s) between the slots and the length of radiation slot (l_1) are less than one free-space wavelength so as to minimize the grating lobes in both E- and H-plane. As shown in Fig. 2(c), two sets of perturbation stubs with the dimensions of (w_x, l_y) and (w_y, l_x) are employed in the backed cavity to suppress unwanted higher order modes. The coupling slot is designed to maximize the power coupled from the feed waveguide to the backed cavity. An impedance matching structure cascaded with the ridge-waveguide structures, as shown in Fig. 2(d), is used in the feed waveguide in layer M5.

C. Taylor synthesis

To achieve the Taylor distribution, the theoretical amplitude of the excitation at each slot is given by [27]

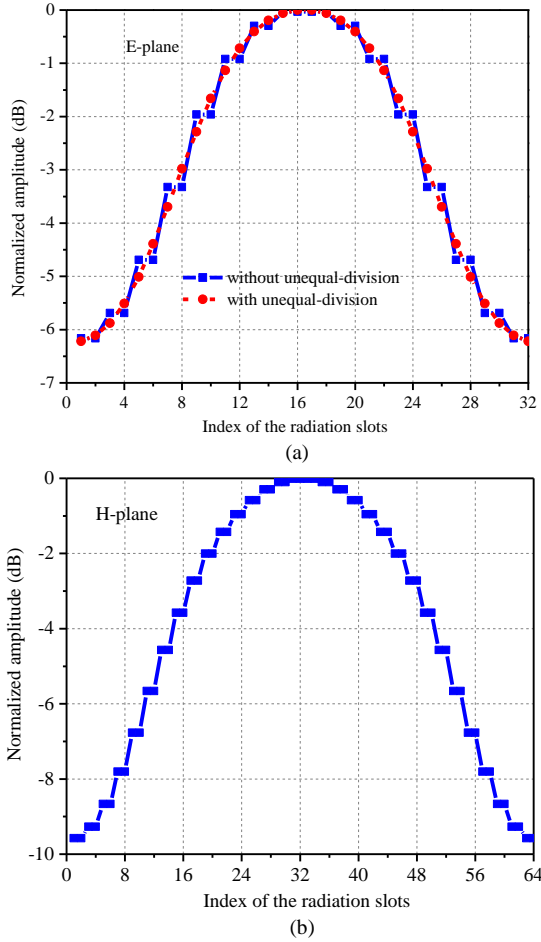$$I_n\left(z_n\right)=1+2\sum_{m=1}^{\overline{N}-1}\overline{S}\left(m\right)\cos\left(mp\right) \tag{1a}$$

Fig. 4. Calculated normalized amplitude distributions for Taylor synthesis. (a) E-plane; (b) H-plane.

$$\overline{S}(m) =$$

$$\begin{cases} \dfrac{\left[\left(\overline{N}-1\right)!\right]^2}{\left(\overline{N}-1+m\right)!\left(\overline{N}-1-m\right)!} \prod_{n=1}^{\overline{N}-1}\left\{1-\dfrac{m^2}{\sigma^2\left[A^2+\left(n-1/2\right)^2\right]}\right\}, & m \leq \overline{N}-1 \quad (1b) \\[2mm] 0, & m \geq \overline{N} \end{cases}$$

where z_n is the location of each radiation slot, the subscript n is the index number of the radiation slot, $p = (2\pi/N)\left[n-(N+1)/2\right]$ and N is the total number of slots. $\overline{S}(m)$ represents the samples for the Taylor pattern, the constant A is related to the maximum allowed SLL of R_0 in that $\cosh(\pi A) = R_0$. $\overline{N}$ is a constant chosen to be 4 in this design. σ is the scaling factor and given by

$$\sigma = \frac{\overline{N}}{\sqrt{A^2 + \left(\overline{N}-\dfrac{1}{2}\right)^2}} \quad (1c)$$

The proposed array consists of 16×32 subarrays each of 2×2 slots. To suppress the sidelobes in both E- and H-planes, two independent groups of Taylor synthesis are used to achieve a SLL of -20 dB with 32 slots in the E-plane and a SLL of -25 dB with 64 slots in the H-plane. For the H-plane, each row has 32 waveguide excitation ports in the feed network, and the amp-
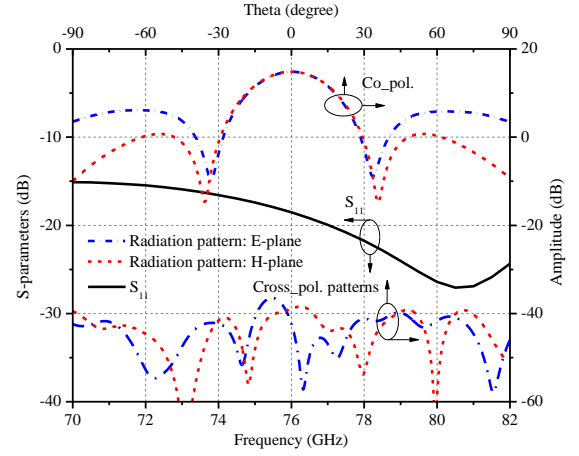

Fig. 5. Simulated reflection, cross polarization and radiation patterns of one 2×2 subarray at 77GHz.

litude complies with a Taylor distribution. However, each of these waveguide ports excite the 2×2 subarray equally along the H-plane. This last-stage simplification makes the amplitude-tapering over the 64 slots slightly different from an ideal Taylor distribution. It becomes a quasi-Taylor distribution. This is to differentiate from the E-plane case, where the amplitude-tapering along the 32 slots complies closely with the Taylor distribution. This is made possible by an unequal power division structure used in the subarray for the E-plane excitation. This structure can be seen from Fig. 2(b). A narrow trench is cut from the underside of layer M2 facing the backed cavity and along the x-axis in each subarray. The dimensions of the trench for each subarray along the x-direction are the same, whereas these are optimized individually along the y-direction. As a result, the amplitude distribution (or power division) at the slots along the y-direction can be adjusted by changing the dimensions of the trench. Fig. 3 shows the variation of the power ratios (between the two slots along the y-direction) with the offset of the trench from the center, rc_m. As shown in Fig. 4(a), this unequal power division helps to smooth the amplitude distribution across the 32 slots in the E-plane. It is worth mentioning that Fig. 4 is calculated from (1a) - (1c). Fig. 4(b) shows the normalized amplitude distribution across the 64 slots in the H-plane. Since there are larger number of radiators in this dimension, the discontinuity in the amplitude distribution is less pronounced. Therefore, unequal power division is not used in the subarray, which results in the quasi-Taylor distribution. This has proven to be sufficient in suppressing the SLL as will be shown later.

Fig. 5 shows the simulated refection coefficient and radiation performance of one subarray with a power ratio of 0.2 dB in the E-plane at 77 GHz. The reflection coefficient is better than -15 dB over the frequency range of 71-81 GHz. The SLL is about -13 dB / -15.5 dB at the E- and H-plane. The cross-polarization level is better than -37 dB. The optimized parameters of this subarray are summarized in Table I. It should be noted that different power ratios may be required for the subarrays along the E-plane, as indicated in the smoothed amplitude distribution in Fig. 4(a). So, rc_m should be optimized for each one of the subarrays along the y-axis.
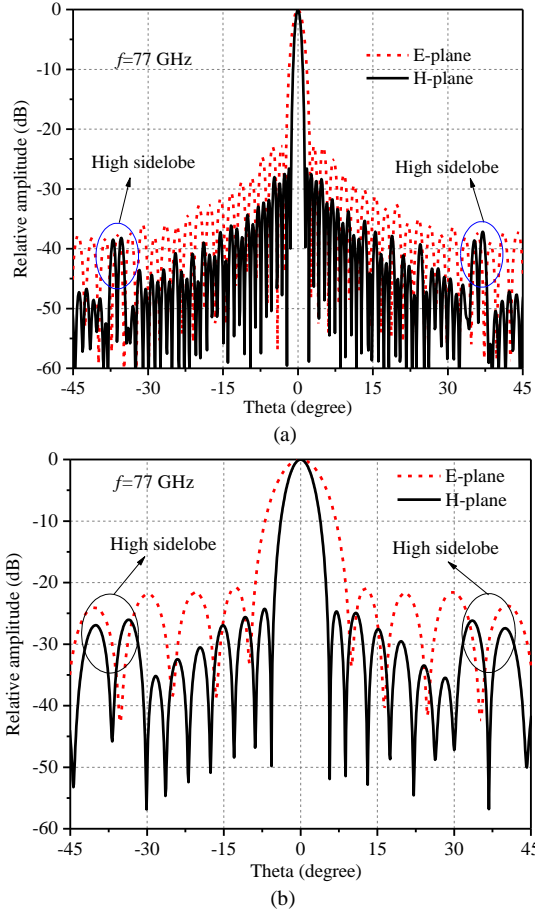
(a)

(b)

Fig. 6. Synthesized radiation patterns. (a) 16×32 subarray antenna; (b) 4×8 subarray antenna.

TABLE I

DIMENSIONS OF THE 2×2- ELEMENT SUBARRAY (UNIT: mm).

h_1	h_2	h_3	h_4	h_5
1	0.8	0.7	1	1
w_1	w_2	w_3	l_1	l_2
1.84	0.8	1.2	2.8	2.8
l_3	rc_w	rc_h	rc_m	bc_w
3.2	0.4	0.3	0.08	4.2
bc_l	w_x	l_y	w_y	l_x
6.1	0.5	0.44	1.3	0.66
rid_h_2	st_w	st_h	po_w	po_l
0.34	0.6	0.4	0.84	0.9
s	a	b	rid_h	rid_w
3.4	1.8	1	0.5	0.4

The synthesized radiation patterns from the amplitude distribution given in Fig. 4 are shown in Fig. 6(a). It can be seen that the 3-dB beam-widths are 2° and 1.1° in the E- and H-plane, while the SLLs are below -22.8 dB and -26.6 dB. The beam-widths and SLLs in the E- and H-plane are independently controlled by the 2-D Taylor-distribution and the different numbers of subarrays along *y*- and *x*-directions. The 3-dB beam-width is ultra-narrow in this design. A wider beam-width can be achieved by reducing the numbers of subarray, while the SLLs can be optimized by using the same method of Taylor synthesis. Fig. 6(b) shows the synthesized radiation patterns of a smaller 4×8 subarray antenna. The 3-dB beam-widths are 8.6° and 4.8° in the E- and H-plane, and the SLLs remain below
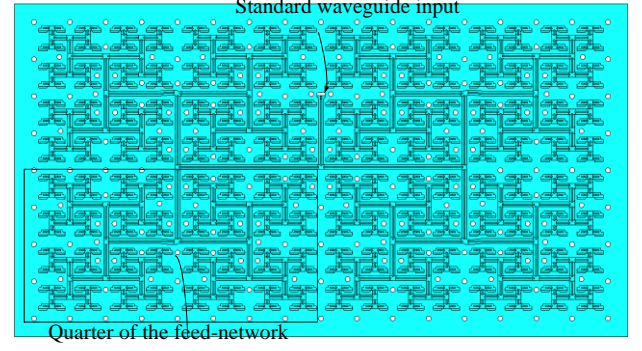

Fig. 7. 16×32 full-corporate single ridge-waveguide feed network.
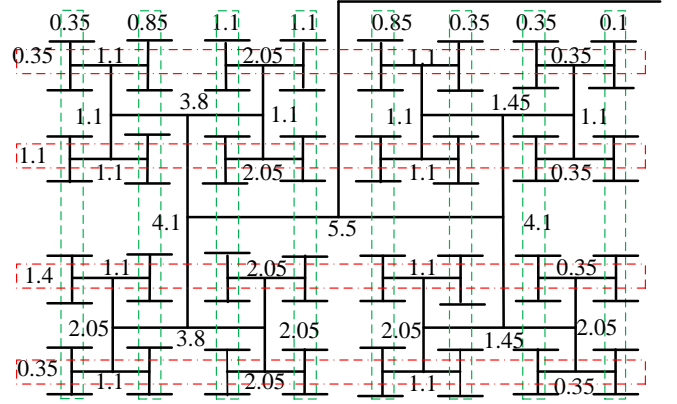
Fig. 8. Calculated power ratios in dB to achieve the Taylor synthesis.

(a)   (b)
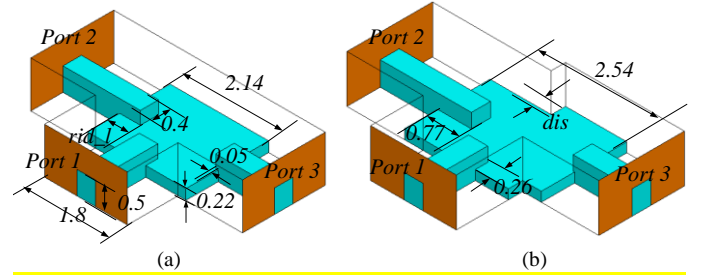
Fig. 9. (a) Basic T-junction unequal power divider; (b) modified unequal T-junction power divider with phase compensation (*rid_l* = 0.55, *dis* = 0.3, unit: mm). Note that the blue parts (grey in black and white print) are metal, showing the structures inside the waveguide. For clarity, the waveguide walls are only shown using frame lines.

-21.1 dB and -25 dB. At about θ=±35° in the H-plane, the sidelobes are noticeably raised, which does not occur in the E-plane. This is a result of the quasi-Taylor amplitude distribution in the H-plane [23].

D. Feed network

Now we will discuss how the 2-D Taylor amplitude tapering is implemented by the feed network. A full-corporate single-ridge waveguide network is used, as shown in Fig. 7. Multiple H-plane T-junction power dividers with different power ratios are used to construct the Taylor amplitude distribution with identical phases. Due to its symmetry, the feed network can be divided into four repeated quarters. From the targeted Taylor synthesis in Fig. 4, the required power ratios of all the H-plane power dividers can be derived, as given in Fig. 8. Those ratios that are very close to each other have been

merged

Fig. 10. (a) Effect of *rid_l* on power ratio; (b) Simulated S-parameters and phase imbalance of the 4.1 dB power divider.

Fig. 11. (a) Effect of *dis* on the phase imbalance; (b) Simulated phase imbalance and S-parameters of the 5.5 dB unequal power divider with phase compensation.
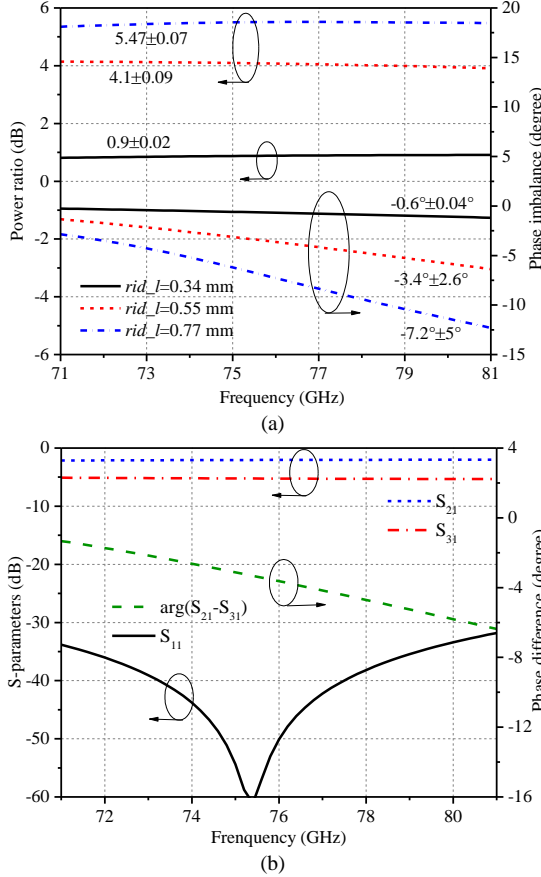

Fig. 12. Simulation power ratios of the nine types of power dividers.

to simplify the implementation. It is worth reiterating that the last stage of the Taylor distribution for the E-plane is realized in the subarrays, not in the feed network.

The feed network requires nine different power ratios: 0.1, 0.35, 0.85, 1.1, 1.45, 2.05, 3.8, 4.1 and 5.5 dB. These are realized by single-ridge H-plane T-junctions. One is shown in Fig. 9(a). A capacitive metal plate is embedded in each of the H-plane T-junction to achieve a wideband impedance matching. The power division ratio can be controlled by the amount of the extrusion of the ridge at one of the output branches, *rid_l*. The variation of the power ratio with *rid_l* is shown in Fig. 10(a) together with corresponding phase imbalance between the outputs. Fig. 10(b) shows the simulated S-parameters of a 4.1 dB unequal power divider. Over the entire operating bandwidth, the power ratio is kept within 4.1±0.09 dB. The reflection coefficient is better than -33 dB.

From Fig. 10(a), it can also be seen that the phase imbalance increases with increasing power ratios. This is mainly due to the unequal length of the metal ridges at the output ports. For the 5.5 dB power divider, the phase imbalance increases to -7.2° at the center frequency with a variation of ±5°. To reduce this phase imbalance, a phase compensation technique is applied. As shown in Fig. 9(b), this is achieved by staggering the output ports by a certain distance, *dis*. Fig. 11(a) demonstrated the effects of *dis* on the output phase imbalance. Fig. 11(b) shows the simulated results of the 5.5 dB unequal power divider after phase compensation. With *dis*=0.3 mm, the phase imbalance is reduced from 7.2°±5° to 0°±2.7°, while the transmission and reflection coefficients remain good.

The simulation results of the desired nine power ratios are shown in Fig. 12. Over the frequency range of 71-81 GHz, the maximum amplitude variation is ±0.09 dB occurring at the power ratios of 3.8 dB and 4.1 dB.

III. EXPERIMENTAL RESULTS

The five layers of the antenna are fabricated separately out of aluminum by CNC machining and assembled by means of screws. The radius of the rounded corners, as defined by the milling tool, is 0.2 mm. During assembly, a set of screws are placed around the antenna to suppress wave leakage. Oxidation
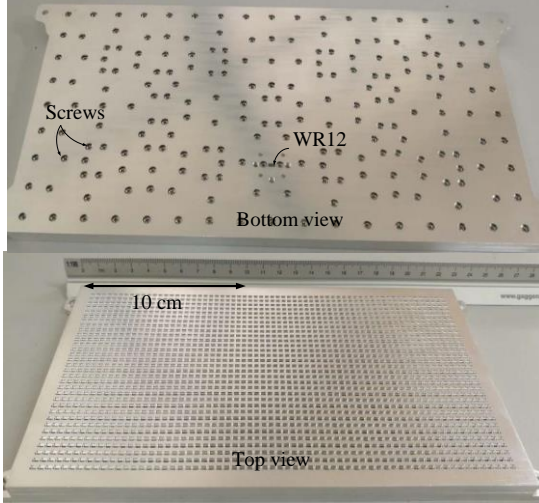
Fig. 13. Photo of the fabricated antenna array.
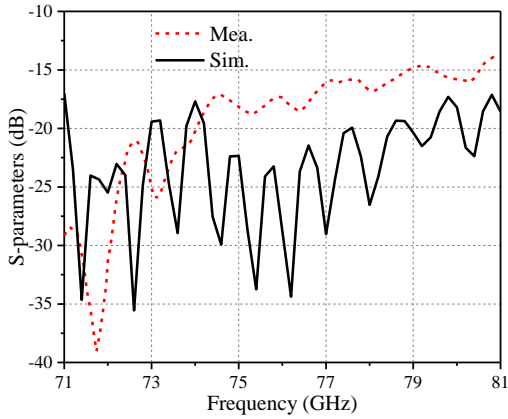
Fig. 14. Measured S_{11} of the proposed array in comparison with simulation.

may affect the performance of the antenna over time. In this work, the antenna is only for verification. Electroplating could be used to protect the antenna from oxidation. The overall size of the prototype is 220 mm × 110 mm × 11 mm. The photograph of the fabricated array is shown in Fig. 13. The radiation performances are measured using an MVG (Microwave Vision Group) compact-range antenna test systems. The nominal dynamic range of the system is 80 dB (over 70 dB in the E-band) and the distance between the antenna under test and the reflector is 2072 mm.

A. Reflection coefficient

The reflection coefficient is measured using AV3672B vector network analyzer, is shown in Fig. 14. A reasonable agreement is obtained on the return loss level between the simulations and the measurements. The reflection coefficient is better than -14 dB between 71 GHz and 81 GHz (a fractional bandwidth of 13%). The large ripple in the simulated reflection coefficient is due to the multiple reflections in the feeding network. In the measurement, the ripple is less pronounced and this is believed to be due to the damping effect by the higher-than-expected losses in the waveguide.
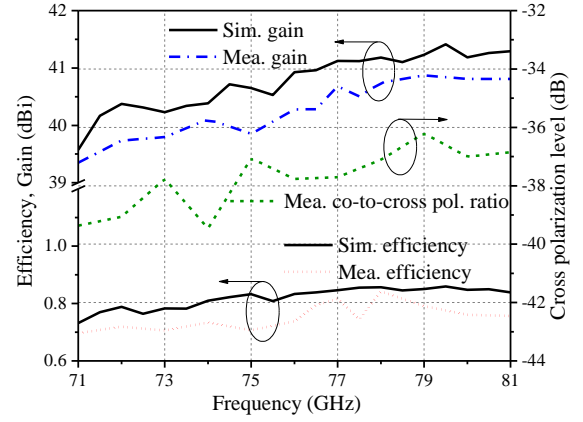

Fig. 16. Frequency dependence of gain, efficiency, and cross-polarization discrimination (XPD).

TABLE II
MEASURED PERFORMANCE OF THE PROPOSED ANTENNA IN COMPARISON WITH SIMULATIONS

Frequency (GHz)	First SLL (dB)		3-dB Beam Width (°)	
	E-plane	H-plane	E-plane	H-plane
	Meas./Sim.	Meas./Sim.	Meas./Sim.	Meas./Sim.
71	-19.5/-20.2	-25/-26	2.3/2.2	1.3/1.3
77	-19.1/-21.2	-29.7/-24	2.1/2	1.1/1.1
81	-18.9/-23.2	-24/-24.3	2/2	1.1/1.1

B. Radiation performances

The simulated and measured normalized radiation patterns in the E- and H-planes at 71 GHz, 77 GHz and 81 GHz are presented in Fig. 15. A very good agreement is obtained between the simulated and measured results, where the patterns almost superimpose. The slight difference in the SLLs can be attributed to fabrication tolerance of the amplitude-tapering feed-network and assembly errors. The E- and H-plane patterns are controlled by different non-uniform aperture distributions imposed on the radiating slots. Therefore, at the same frequency, the SLLs and the 3-dB beam-width of the E- and H-plane are different. The simulated and measured first SLLs and the 3-dB beam-widths are detailed in Table II. Over the operating bandwidth, the measured first SLLs are below -18.9 dB / -24 dB in the E- and H-plane, respectively. The maximum beam width is 2.3° / 1.3°. At 77 GHz, the 3-dB beam-width is 2.1° / 1.1°. As expected, two raised sidelobes appear at about θ=±37° because of the quasi-Taylor amplitude distribution for the H-plane, as shown in Fig 15. Still these are lower than the first side lobes.

Fig. 16 plotted the measured peak gain and the cross-polarization at θ=0° as a function of frequency. The measured maximum peak gain is 40.9 dBi at 79 GHz. Over the desired frequency range, the peak gain is over 39.4 dBi, which is about 0.5 dB lower than the simulation. This small discrepancy comes from the milling process and assembly imperfection, when surface roughness and discontinuity between layers could have caused extra power losses. The measured antenna efficiency of better than 70% is achieved over the whole frequency band. Fig. 16 also shows a very low cross-polarization discrimination (XPD) of -36.2 dB over the operating bandwidth.
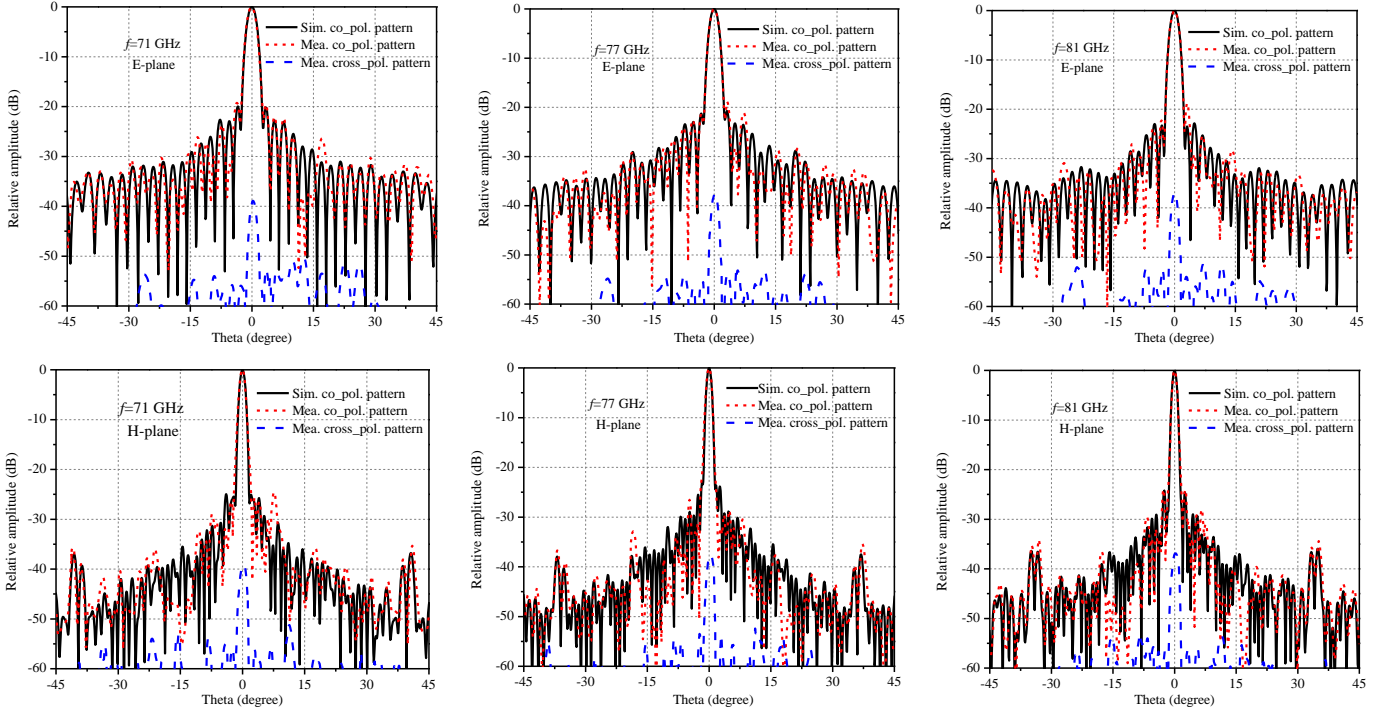
Fig. 15. Normalized co-pol and cross-pol radiation patterns in E-plane and H-plane at 71, 77 and 81 GHz.

TABLE III
COMPARISON OF AMPLITUDE TAPERING ARRAYS

Ref.	Center frequency (GHz)	Method	No. elements	Peak gain (dBi)	SLL (dB)	3-dB beam-width (degree)	Cross-polarization discrimination (dB)
[16]	24	Dolph–Chebychev synthesis	10	14.5	E-plane: -15 H-plane: N/A	E-plane:10 H-plane: N/A	-23
[19]	9	Differential evolution algorithm	10	14.5	E-plane: -21.3 H-plane: N/A	E-plane:8.3 H-plane: N/A	-25
[21]	77	Taylor synthesis	N/A	29.9	E-plane: -18.1 H-plane: -18	E-plane:4.8 H-plane:4.6	N/A
[23]	15	Taylor synthesis	64	29.5	E-plane: -22 H-plane: -22	E-plane:5.5 H-plane:5.3	-40
This work	77	Taylor synthesis both in E- and H-plane	512	39.4	E-plane: -18.9 H-plane: -24	E-plane:2.3 H-plane:1.3	-36.2

C. Comparison

The performance of this prototype array has been compared with several other published amplitude-tapering arrays in Table III. This work is the first reported array with 2D Taylor distribution. It achieved the peak gain of 39.4 dBi with 512 subarrays and a competitively low side lobe level. The achieved cross-polarization discrimination is also very low. With the 2-D Taylor synthesis and different array dimensions along the *x* and *y* direction, the radiation performances in the E- and H-plane can be independently controlled.

IV. CONCLUSION

This paper presents a high gain 32×64-element SW array with unequal beam-width in the E- and H-planes and very low SLLs over the band of 71-81 GHz. A 2-D Taylor synthesis has been implemented in the transverse and longitudinal directions to independently control the SLLs and 3-dB beam-widths. This feature is important for vehicular communications and radar applications. For demonstration purpose, an experimental prototype has been designed, fabricated and measured. The experimental results show the proposed array has a 3-dB beam-width of 2.1°/1.1° and SLLs of -19.1 dB/-29.7 dB in the E- and H-plane at 77 GHz. The peak gain is more than 39.4 dBi

and the <mark>cross-polarization discrimination</mark> is better than -36.2 dB. With these unique features and high performance, the demonstrated antenna could find applications in vehicular radars as well as multi-Gbps wireless communication systems.

REFERENCES

[1] W. Menzel, A. Moebius, "Antenna concepts for millimeter-wave automotive radar sensors," *Pro. IEEE,* vol. 100, pp. 2372–2379, Jul. 2012.

[2] J. Xu, W. H., H. Zhang, G. Wang, Y. Yu, and Z. H. Jiang, "An array antenna for both long- and medium-range 77 GHz automotive rdar applications," *IEEE Trans. Antennas Propag.,* vol. 65, no. 12, pp. 7207 – 7216, Dec.2017.

[3] C. Vasanelli, F. Bogelsack and C. Waldschmidt, "Reducing the radar cross-section of microstrip arrays using AMC structures for the vehicle integration of automotive radars," *IEEE Trans. Antennas Propag.*, vol. 66, no. 3, pp. 1456 – 1464, Mar.2018.

[4] J. Hasch, E. Topak, R. Schnabel, T. Zwick, R. Weigel, and C. Waldschmidt, "Millimeter-wave technology for automotive radar sensors in the 77 GHz frequency band," *IEEE Trans. Microw. Theory Techn.,* vol. 60, no. 3, pp. 845 – 860, Mar. 2012.

[5] M. E. Eltayeb, J. Choi, T. Y. Al-Naffouri and R. W. Heath, Jr., "Enhancing secrecy with multiantenna transmission in millimeter wave vehicular communication systems," *IEEE Trans. Veh. Technol.,* vol. 66, no. 9, pp. 8139–8151, Sep. 2017.

[6] C. X. Mao, S. Gao, Y. Wang, "Dual-band full-duplex Tx/Rx antennas for vehicular communications," *IEEE Trans. Veh. Technol.,* vol. 67, no. 5, pp. 4059–4070, May. 2018.

[7] Y. Cui, X. Fang, L. Yan, "Hybrid spatial modulation beamforming for mmwave railway communication systems," *IEEE Trans. Veh. Technol.*, vol. 65, no.12, pp. 9597-9606, Dec.2016.

[8] L. Yang, Y. Zeng, R. Zhang, "Channel estimation for millimeter wave MIMO communications with lens antenna arrays," *IEEE Trans. Veh. Technol.*, vol. 67, no. 4, pp. 3239–3251, Apr. 2018.

[9] Electronic Communications Committee (ECC) Recomm-endation (05)07 "Radio frequency channel arrangements for fixed service systems operating in the bands 71-76 GHz and 81-86 GHz" Revised Dublin 2009.

[10] Z. C. Hao, M. He, K. K. Fan, and G. Luo, "A planar broadband antenna for the E-Band gigabyte wireless communication," *IEEE Trans. Antennas Propag.*, vol. 65, no. 3, pp. 1369–1373, Mar. 2017.

[11] H. A. Diawuo, S. J. Lee and Y. B. Jung, "Sidelobe-level reduction of a linear array using two amplitude tapering techniques," *IET Microw. Antennas Propag.*, vol. 11, lss.10, pp. 1432–1437, Aug. 2017.

[12] M. N. Ranjani and B. Sivakumar, "Design & analysis of rectangular microstrip patch antenna linear array using binomial distribution," in *Proc. 3th Int. Conf. on Electrical, Electronics, Computer Engineering and their Applications (EECEA),* Apr. 2016, pp. 12-17.

[13] N. K. Mishra and S. Das, "Investigation of binomial & chebyshev distribution on dielectric resonator antenna array," in *Proc. Int. Conf. on Electronic Systems, Signal Processing and Computing Technologies,* Jan. 2014, pp. 434-437.

[14] T. T. Taylor, "Design of line-source antennas for narrow beamwidth and low sidelobes," *IRE Trans. Ant.& Prop.,* vol. AP-3, pp. 16–28, Jan. 1955.

[15] R. C. Hansen, "Contributions of T.T. Taylor to array synthesis," in *Proc. IEEE Antennas and Propagation Society Int. Symp.,* Jul. 1999, vol. 4, pp. 2294–2297.

[16] G. F. Hamberger, S. Trummer, U. Siart, T. F. Eibert, "A planar dual-polarized microstrip 1-D-beamforming antenna array for the 24-GHz band," *IEEE Trans. Antennas Propag.*, vol. 65, no. 1, pp. 142-149, Jan. 2017.

[17] S. Ogurtsov, S. Koziel, "Sidelobe reduction in linear antenna arrays with corporate-feeds of non-uniform power distribution," in *Proc. 11th Euro. Conf. on Antennas and Propagation (EUCAP),* Mar. 2017, pp. 3259 – 3263.

[18] T. Varum, J. N. Matos, P. Pinho, R. Abreu, "Nonuniform broadband circularly polarized antenna array for vehicular communications," *IEEE Trans. Veh. Technol.,* vol. 65, no.9, pp. 7219-7227, Sep.2016

[19] J. Yin, Q. Wu, C. Yu, H. Wang, W. Hong, "Low-sidelobe-level series-fed microstrip antenna array of unequal interelement spacing," *IEEE Antennas and Wire. Propag. Lett.,* vol. 16, pp. 1695-1698, Feb. 2017

[20] Y. Tyagi, P. Mevada, S. Chakrabarty, R. Jyoti "High-efficiency broadband slotted waveguide array antenna," *IET Microw. Antennas Propag.*, vol. 11, lss. 10, 1401 – 1408, Aug. 2017.

[21] J. Hirokawa, M. Ando, "Sidelobe suppression in 76-GHz post-wall waveguide-fed parallel-plate slot arrays," *IEEE Trans. Antennas Propag.,* vol. 48, no. 11, pp. 1727 – 1732, Nov. 2000.

[22] T. P. Potelon,M. Ettorre, L. L. Coq, T. Bateman, J. Francey, D. Lelaidier, E. Seguenot, F. Devillers, R. Sauleau, "Continuous transverse stub array for Ka-band applications," *IEEE Trans. Antennas Propag.*, vol. 65, no. 12, pp. 6307–6316, Dec. 2017.

[23] G. L. Huang, S. G. Zhou, T. H. hio, H. T. Hui, and T. S. Yeo, "A low profile and low sidelobe wideband slot antenna array feb by an amplitude-tapering waveguide feed-network" *IEEE Trans. Antennas Propag.*, vol. 53, no. 1, pp. 419–423, Jan. 2015.

[24] T. Tomura, J. Hirokawa, T. Hirano, M. Ando, "A 45° linearly polarized hollow-waveguide 16 ×16-Slot array antenna covering 71–86 GHz Band," *IEEE Trans. Antennas Propag.,* vol. 62, no. 10, pp. 5061 – 5067, Oct. 2014.

[25] Y. Miura, J. Hirokawa, T. Hirano, M. Ando, Y. Shibuya, G. Yoshida "Double-layer full-corporate-feed hollow-waveguide slot array antenna in the 60-GHz band," *IEEE Trans. Antennas Propag.,* vol. 59, no. 8, pp. 2844 – 2851, Aug. 2011.

[26] D. M. Pozar, "Microwave enginneering", 3rd edition, John Wiley & Sons, 2012.

[27] C. A. Balanis, "Antenna theory: analysis and design", 3rd edition, John Wiley & Sons, 2005.